A Molecular Electronic Transducer based Low-Frequency

Accelerometer with Electrolyte Droplet Sensing Body

by

Mengbing Liang

A Thesis Presented in Partial Fulfillment
of the Requirements for the Degree
Master of Science

Approved May 2013 by the
Graduate Supervisory Committee:

Hongyu Yu, Chair
Michael Kozicki
Hanqing Jiang

ARIZONA STATE UNIVERSITY

August 2013

ABSTRACT

"Sensor Decade" has been labeled on the first decade of the 21st century. Similar to the revolution of micro-computer in 1980s, sensor R&D developed rapidly during the past 20 years. Hard workings were mainly made to minimize the size of devices with optimal the performance. Efforts to develop the small size devices are mainly concentrated around Micro-electro-mechanical-system (MEMS) technology. MEMS accelerometers are widely published and used in consumer electronics, such as smart phones, gaming consoles, anti-shake camera and vibration detectors.

This study represents liquid-state low frequency micro-accelerometer based on molecular electronic transducer (MET), in which inertial mass is not the only but also the conversion of mechanical movement to electric current signal is the main utilization of the ionic liquid. With silicon-based planar micro-fabrication, the device uses a sub-micron liter electrolyte droplet sealed in oil as the sensing body and a MET electrode arrangement which is the anode-cathode-cathode-anode (ACCA) in parallel as the read-out sensing part. In order to sensing the movement of ionic liquid, an imposed electric potential was applied between the anode and the cathode. The electrode reaction, $I_3^- + 2e^- \leftrightarrow 3I^-$, occurs around the cathode which is reverse at the anodes. Obviously, the current magnitude varies with the concentration of ionic liquid, which will be effected by the movement of liquid droplet as the inertial mass. With such structure, the promising performance of the MET device design is to achieve $10.8\ \mathrm{V/G}\ (\mathrm{G} = 9.81\ \mathrm{m/s^2})$ sensitivity at 20 Hz with the bandwidth from 1Hz to 50 Hz, and a low noise floor of $100\ \mu\mathrm{g}/\sqrt{\mathrm{Hz}}$ at 20 Hz.

ACKNOWLEDGMENTS

I wish to thank my advisor Dr. Hongyu Yu for the support and help on this research project, as well as all my committee members. I am also pleased to have this opportunity to thank my colleagues Hai Huang, Rui Tang, Teng Ma, Ruirui Han, Bryce Carande and Jon Oiler for all of the help. The work was majorly supported by NASA-PIDDP-NNX10AL25G (USA).

Finally, I would like to thank my parents, for their support and encouragement.

TABLE OF CONTENTS

Page

LIST OF TABLES iv

LIST OF FIGURES v

CHAPTER

1 INTRODUCTION 1

1.1 Introduction to Recent MEMS Accelerometers 1

1.2 Introduction to Typical MEMS Process 6

1.3 Introduction to Integrated System of MEMS 10

2 OPERATION PRINCIPLE AND FABRICATION PROCESS 13

2.1 Structures of MET Accelerometer 13

2.2 Principle of Droplet Movement 16

2.3 Principle of Electrochemical Reation 17

2.4 Fabrication Process 19

3 PERIPHERAL CIRCUITS DESIGN 22

3.1 Circuit Design for The Signal Analysis 22

3.2 Temperature Compensation 24

4 TEST AND RESULTS 26

4.1 Test Setup 26

4.2 Experimental Results 27

4.3 Noise Analysis and Improvement 30

REFERENCES 33

LIST OF TABLES

Table Page

1. System Planning Corporation Market Survey(1999) with 1996 product volume and a forecast of 2003 sales (in millions of US$) [3] 2

2. Self noise analysis of test equipment 30

3. Noise floor with different gain 32

LIST OF FIGURES

Figure Page

1. Analog Devices ADXL-50 Die Photo. (Source: Analog Devices) 3

2. Differential Capacitors inside ADXL Accelerometer 4

3. Block Diagram of ADXL integrated system.. 4

4. Top & Cross view of piezoresistivity accelerometer 5

5. Piezoresistivity accelerometer with DRIE (a) The design and principle demotions (b) SEM diagraph of a flexure (Source: [4]) 5

6. Devices design flow with key factors 6

7. Process of optical lithography and silicon dioxide etching 9

8. Lift-off process 9

9. Soft Lithography Pattern 10

10. Structure of a MOS device 11

11. Structure of Transimpedance amplifier 12

12. Structure of Instrument amplifier 12

13. Traditional MET accelerometer 14

14. Droplet MET accelerometer 15

15. Distribution of the concentration of electrolyte 17

16. Fabrication Process Flow 19

17. Overview of the electrolyte droplet-based MET accelerometer 21

18. Schematic of peripheral circuit 22

19. Biasing circuit for temperature compensation [14] 24

20. Overview of the PCB board 26

21. Test Setup Schematic 27

22. Measurement result of sensitivity of the MET accelerometer at 20 Hz 28

23. Measurement result of sensitivity frequency response of the droplet-based micro MET accelerometer 29
24. Measured output signal spectrum under a 0.35G excitation at 20Hz 29
25. Noise spectrum of test Circuits 30

Chapter 1

INTRODUCTION

Molecular electronic transducer (MET) belongs to a class of inertial sensors which are widely used as accelerometers, seismometers, tilt sensors and velocity meters. METs capture the signal of the motion of the sensing body from the physical and chemical phenomena caused by the hydrodynamic motion of electrolyte liquid captured by the electrodes. Counts of advantages of MET technology had been discovered in the 1950s, such as high sensitivity, low-noise detection, low-power dissipation and easy fabrication. However, the poor linearity and lack of reproducibility limited the development during the past decades years and sensors with piezoelectric material was applied to mass and inertial applications instead. Nevertheless, low frequency signals from the earthquake, storm and industrial manufacture are difficult to be detected by piezoelectric material based sensors. As the result, researches on the low frequency signal recalls the MET technology and it has been proved its low frequency performance is unexpected good. [1]

1.1 Introduction to Recent MEMS Accelerometers

Accelerometer which is also named, inertial sensor, is a device which measures the proper acceleration, which is acceleration experienced by an object which is relative to a free-fall, inertial or a shock. With an inertial movement by the force on the frame, mechanical drift will generate relative electrical signal, as accelerometer has the ability to invert the mechanical signal to electrical one. As the acceleration is inverse proportion to the mass of the object which is expressed as,

$$\text{Force} = \text{Mass} \times \text{Acceleroation}$$

The proper mass of the accelerometer will influence the acceleration of the total system which is unacceptable, besides, the sensitivity will also decrease by the increasing of the mass. In terms of the reliability of such inertial device, small sizes will bring lots of benefits.

Performance enhancement of silicon MEMS devices have been proved that MEMS technology will benefit lots on the environment detections as the small sized fabrication. Microsystems have a long history since now, dating back to the earliest days of MEMS. With the development of the integrated circuits in the early 1960s, numbers of laboratories were built to focus on using the same technology on the integrated sensors. The first ideas came from the silicon etching using for the micro-sized pressure sensor. With the demand on improving the vehicle energy saving, MEMS pressure sensor made a spectacular success and low cost and high performance characters bring lots of attentions on MEMS technology. [2]

System Planning Corporation [3] published a survey and a forecast of the sales of MEMS applications. The Table 1.1 presents the result of the survey.

MEMS Device and Applications	1996	2003
Inertial Measurement: Accelerometers and gyros	350-540	700-1400
Microfluidics: Ink-jet printers, mass-flow sensors, biolab chip	400-500	3000-4450
Optics: Optical switches, displays	25-40	440-950
Pressure Measurement: Automotive, medical, industrial	390-760	1100-2150
RF Devices: Cell phone components, devices for radar	N/A	40-120
Other Devices: Microrelays, sensors, disk heads	510-1050	1230-2470

Table 1 System Planning Corporation Market Survey(1999) with 1996 product volume and a forecast of 2003 sales (in millions of US$) [3]

This table indicated that the demands of micro-sensor was huge at 1999 and MEMS technology indeed developed rapidly during the recent two decades. With good CMOS

capability, micro-sensor system made huge success on the market, especially for the ADXL series accelerometers by Analog Devices shown in Figure 1.

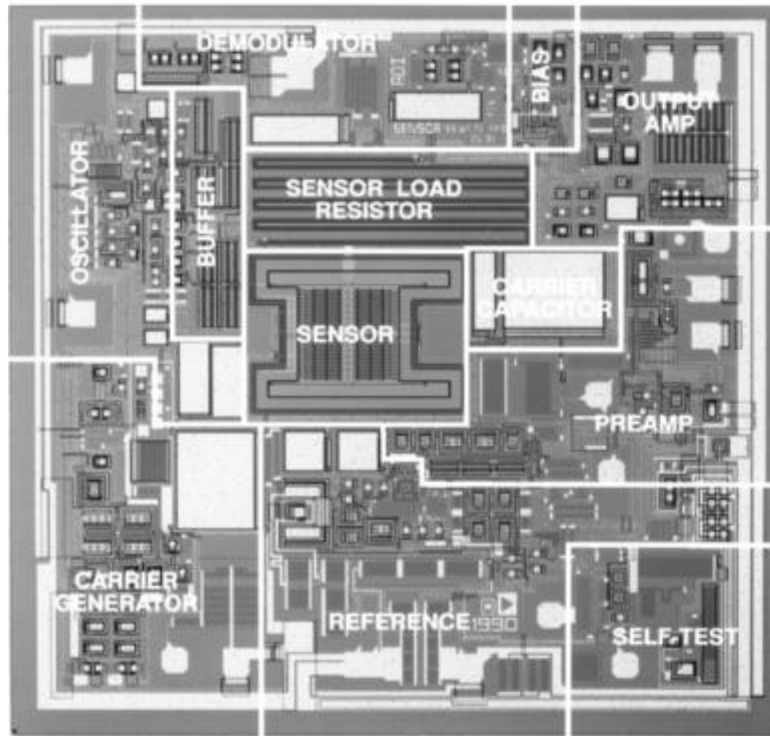

Figure 1 Analog Devices ADXL-50 Die Photo. (Source: Analog Devices)

The mechanical sensor region is in the center of the die which is an array of spring connected cantilever beams. Vibration deliver from the environment to the cantilever beams through the frame of the total system will cause a movement which will vary the displacement of two differential capacitors which will invert to electrical signal as shown in the Figure 2. The proof mass structure will vibrate relative to the fixed block with an excitation through a spring connecting with it. Varies of C1 inverse to C2, as C1 and C2 are fixed the different sides of the proof mass. With a differential amplifier, the acceleration sensitivity will increase and the noise will be cancelled.

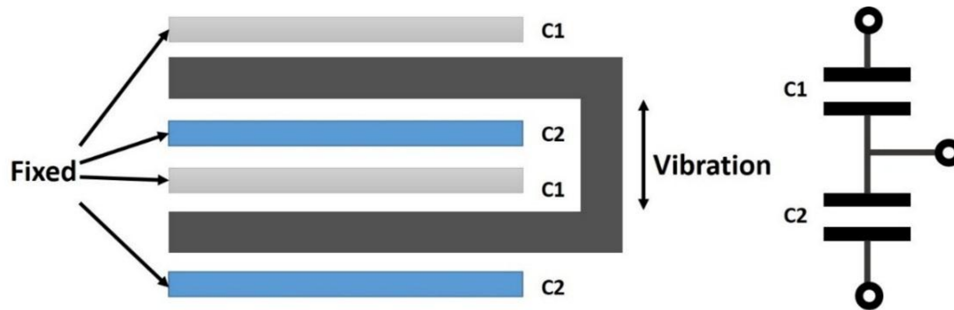

Figure 2 Differential Capacitors inside ADXL Accelerometer

The block diagram of ADXL series accelerometer is shown in Figure 3. This is a close-loop system with a force-feedback which benefits the linearity and accuracy of the system. Comparing with the open-loop system design, sacrifice sensitivity in a tolerance interval and increase the dynamic working bandwidth.

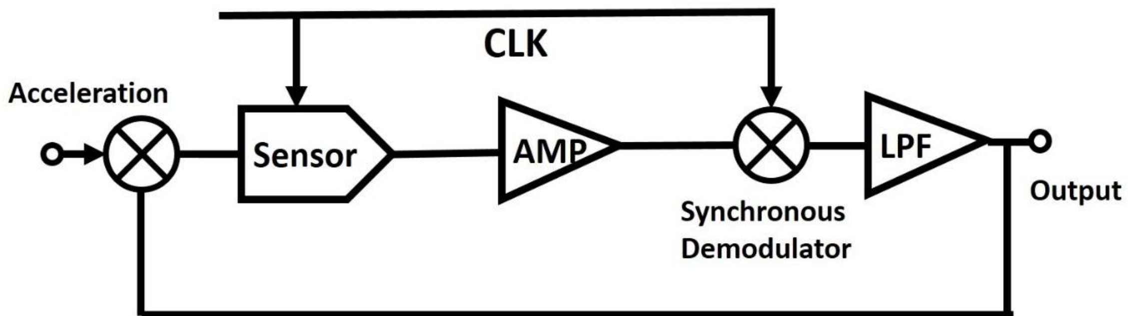

Figure 3 Block Diagram of ADXL integrated system

Piezoresistive accelerometer was another design with MEMS technology which was first described 20 years ago [4] [5]. Piezoresistive accelerometers are usually designed with flexures and proof masses that deflect out-of-plane. With several piezoresistors deposited on the flexures connected as diamond circuit's structure, signal according to the vibration on the proof mass will be inverted to current signal which could be amplified by circuit amplifier. These devices need an air-gap between the cover and the substrate with which the T-shape proof mass is able to vibrate with the acceleration signal as shown in Figure 4.

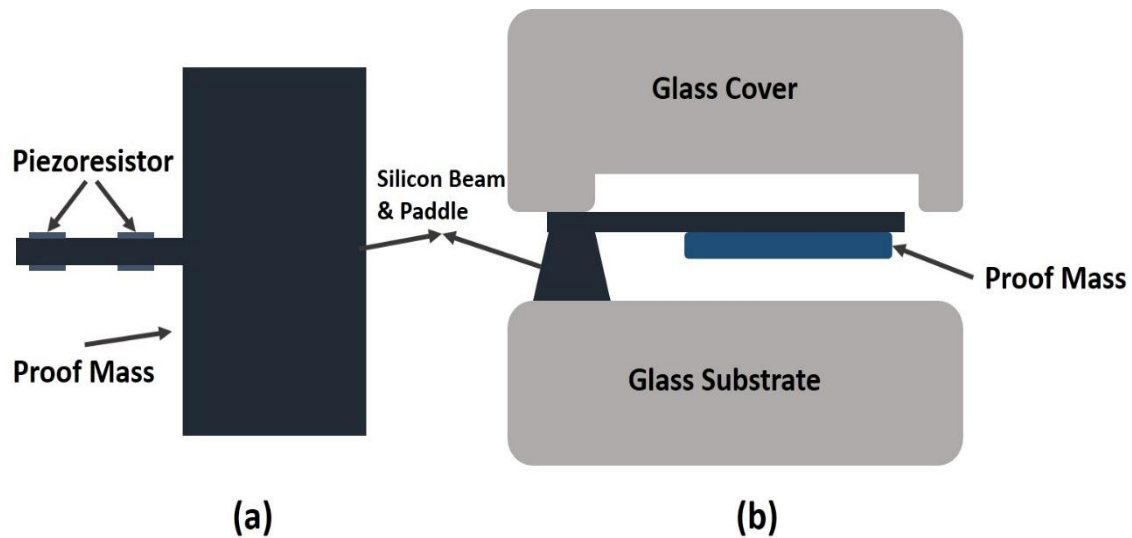

Figure 4 Top & Cross view of piezoresistivity accelerometer

However, the glass to silicon bounding is necessary in the fabrication process which limited the size of the device. With the development of deep reactive ion etching (DRIE), which allows the formation of optimally shaped proof masses are in-plane and flexures stiff out-of-plane as shown in the Figure 5. Multiple shapes and sizes could be fabricated on the silicon substrate, which simplified the process and cost lower.

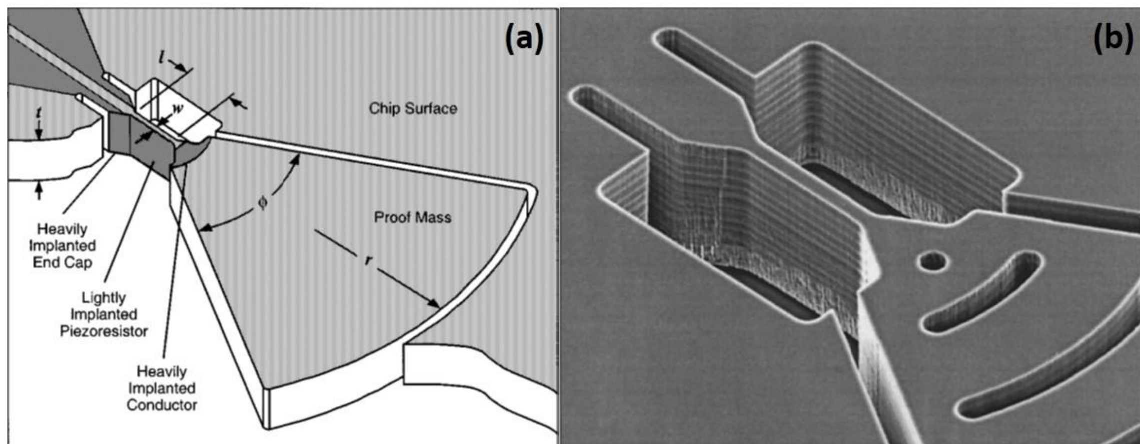

Figure 5 Piezoresistivity accelerometer with DRIE (a) The design and principle demotions (b) SEM diagraph of a flexure (Source: [4])

1.2 Introduction to Typical MEMS Process

There are five highest level issues need to be considered about at the beginning of the design and development of new devices and products, which includes: Market, Impact, competition, technology and manufacturing. “Market-drive design” and “Technology-drive design” provide two different methods evaluating the feasibility of a new project. [6] Market-drive design usually suit for the improvement of a new device in order to fulfil the specific capability at low-cost. Technology-drive design is one for the existing device which the specific properties achieve the market fortunately, which means it is an “opportunistic” design. With a budget control and proper market time, new devices could be commercialized with lots benefits. It is a regular pattern that marketing identification often lags the technology development. As shown in the Figure 6, only considering about every aspects of the influence factors, a new design could have an opportunity to be released.[7]

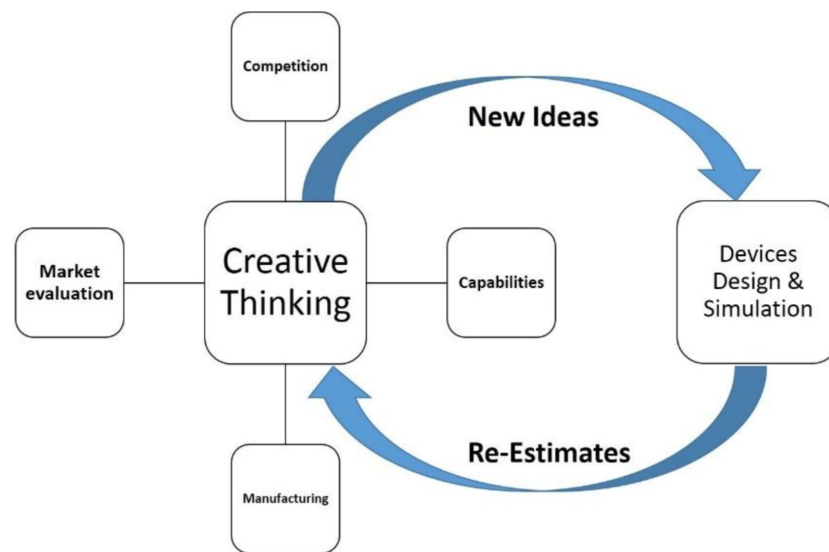

Figure 6 Devices design flow with key factors

Both microelectronics such as CMOS and MEMS fields develop on the

microfabrication, which is based on planar technologies. As the result of investments on the wafer-based process, MEMS designers develop new devices based on the same technologies. As wafer clean, E-beam PVD, LPCVD, Optical lithography, lift-off and soft lithography were used in the fabrication process of MET accelerometer. There would be a brief introduction of those technologies.

Wafer clean can be the first step in microelectronic processes in order to develop a completely clean and flat substrate to prevent the failure or low yield caused by the particles or organic residues. RCA cleans is the standard wafer cleaning steps. With 7:3 mixture of sulfuric acid and hydrogen peroxide, all organic coatings need be removed in strong oxidant firstly. Then organic residues should be removed by a 5:1:1 mixture with water, hydrogen peroxide and ammonium hydroxide. However, a thin silicon dioxide film could be grown as the strong oxidizing, a dilute hydrofluoric acid etch would be provided. Finally, ionic clean will be provided to remove the ionic contaminants. As the organic residues would be difficult to remove, RCA cleans must be done before high temperature process such as oxidation and ion implantation.

Thin film pattern is involved almost every MEMS devices process which includes, physical vapor deposition, chemical vapor deposition, electro-planting, spin casting and gel-deposition. Physical vapor deposition (PVD) is used primarily for metals deposition which includes two major methods: evaporation and sputtering. The metal would be placed in a crucible and heated by an incident electron. The metal vapor would be absorbed on the wafer. All the procedure should be done under high-vacuum circumstance or thin layer would be pilt-off. With the characteristics of directional and allowing shadowing effects, E-beam PVD usually used in accelerometers deposition.

Chemical vapor deposition (CVD) is a class of deposition way with precursor materials heated in a furnace. Chemical reaction occurs on the surface of the wafer and compound will be deposited on it. On the contract from PVD, CVD process is typically provided under low pressure conditions and an inert diluent gas, such as nitrogen is usually added. Low-pressure CVD and plasma-enhanced CVD are the typical methods with CVD technologies. Although CVD provides variety of material deposition, most the processes need be under high temperature circumstance which is above at least 400 centigrade. As the result, CVD generally is provided at the first step. Comparing to the thermal oxidation, LPCVD generates more voids, which, in turn, has fewer voids than PECVD.

Similar to the film developing, optical lithography utilize the photosensitivity of enabling material. The enabling material of optical lithography is called photoresist which is a polymeric optically-sensitive liquid material before heated. With controlling the speed of spinning, photoresist will coat on the surface of the wafer uniformly at different thickness which can be at least several micro-meters. Two different types of photoresists are called Negative photoresist which becomes cross-linked and insoluble in the developer after exposed and Positive photoresist which is insoluble before exposed. With a printed or chrome deposited photomask, various shape of patterns could be transferred to the photoresist after a UV exposed. As shown in Figure 7, with a hard baked photoresist after optical exposure, it can be used as covering layer according to its stability.

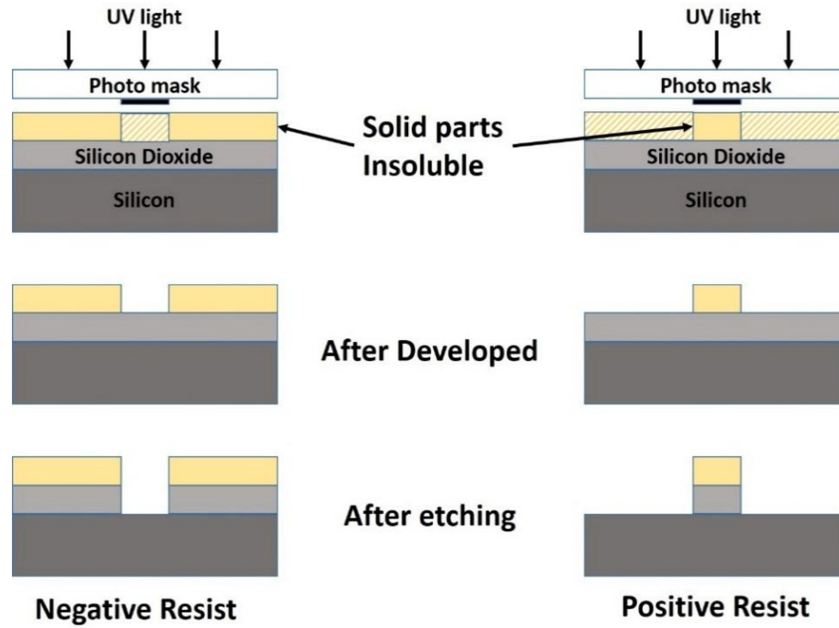

Figure 7 Process of optical lithography and silicon dioxide etching

Besides the covering layer, photoresist can use as a sacrificial layer to transfer the pattern which is called lift-off process. When a wafer is coated with photoresist, exposed and developed, patterns have been transferred onto the photoresist as discussed above. Unlike the metal etching process using the resist as covering layer, metal deposition is provided after the photolithography process. After that, photoresist could be removed with the metal deposited above by organic solvent and the metal above substrate will be left as shown in Figure 8.

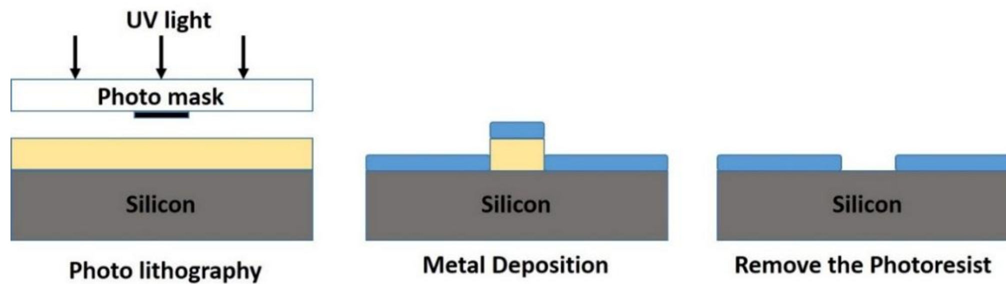

Figure 8 Lift-off process

Unlike traditional optical lithography, soft lithography uses the modeled polymeric object to transfer the pattern which is similar to a stamp pattern on the paper. Silicone rubber and PDMS are the most common used material for soft lithography. [8] When coated the substrate with such patterned soft material, physical etching will be applied to remove the undesired part as Figure 9 shown.

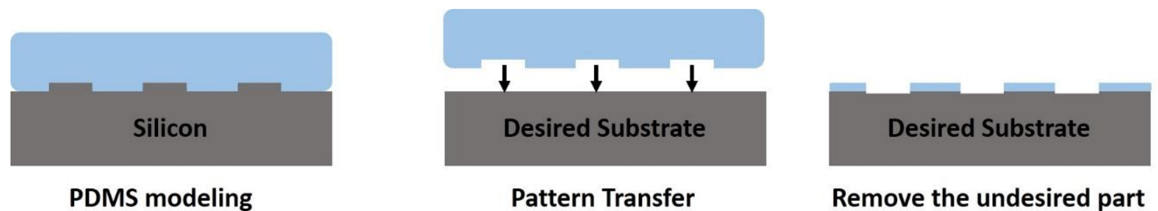

Figure 9 Soft Lithography Pattern

1.3 Introduction to Integrated System of MEMS Devices

According to the introduction to the basic MEMS technologies discussed above, it is obviously lots of MEMS devices are CMOS compatible which means both the device and circuits system can be integrated on one chip. CMOS compatible is an essential issue which even decide the capability to be commercialized. For most sensors, the signal from the environment would be convert to electrical signal which includes current and voltage signal. Although circuits design is a different fields from MEMS design, the method to convert the signal detected by the device to the desired signal, to amplify the desired signal and to reduce the noises from the environment and the device itself. A brief introduction about the CMOS amplifier and some general circuits system will be presented next. [9][10]

Figure 10 shows a structure of a MOS device, which is fabricated on a p-type silicon substrate with two heavily-doped n type regions, in which the boron used as the p type

doping material and phosphorus used for n type doping. A thin layer of silicon dioxide insulating the gate from the silicon substrate and a layer of polysilicon is deposited on top of it. As the high concentration doping of n+ and p+ region needs high temperature circumstance, most MEMS processes have to follow the high temperature ones. However, the metal layer is necessary in CMOS process which can’t stand under high temperature. As the result, the capability to CMOS process is an essential issue.

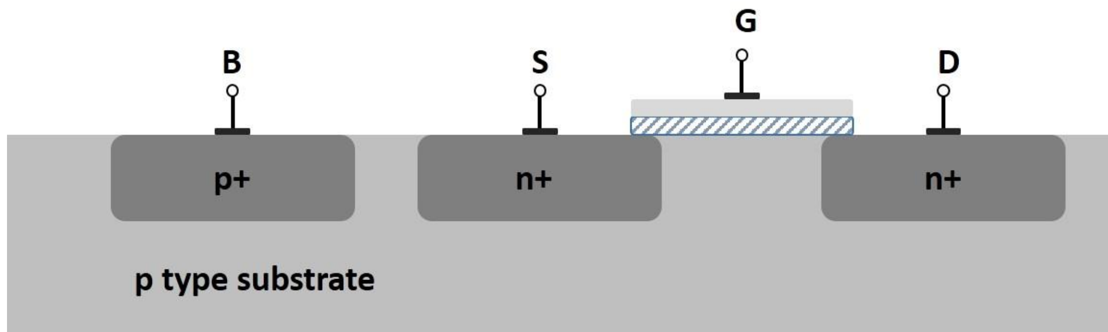

Figure 10 Structure of a MOS device

In electronic circuits design, transimpedance amplifier is an amplifier which converts current to voltage. Generally idea is to use a high value resistance connected with ground to convert the current signal to voltage one. However, the output impedance of the devices may vary at a very high range which will influence the potential on the resistance. As a result, an op-loop amplifier is applied to isolate the input current signal and the voltage output signal as shown in the Figure 11 according to the high input impedance of CMOS amplifier.

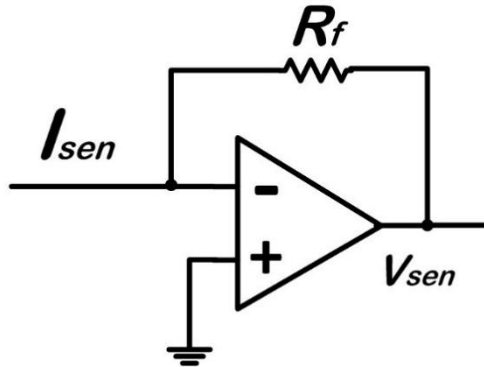

Figure 11 Structure of Transimpedance amplifier

Instrumentation amplifier is a type of differential amplifier outfitted with input buffer, which has a very low DC offset. With low input referred noise and high open-loop gain, instrumentation amplifier has a satisfactory performance when using at MEMS sensors with low power supply. With 3 composed op-amps, it can both fulfill the high input impedance and controllable high gain with adjust the R_{gain} which is shown in Figure 12.

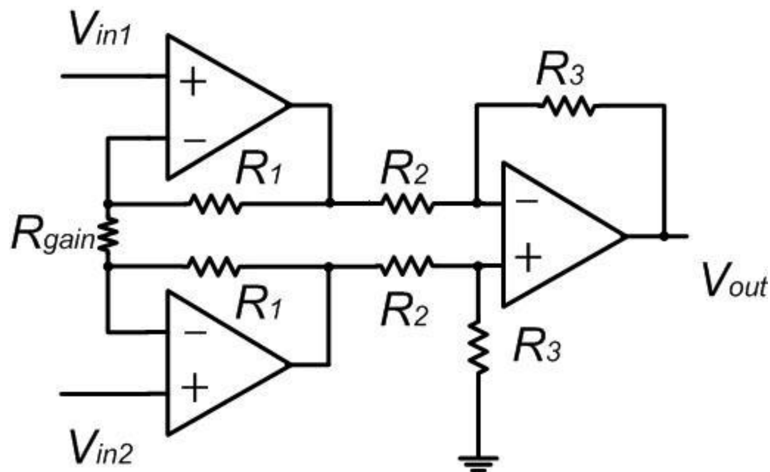

Figure 12 Structure of Instrument amplifier

Chapter 2

OPERATION PRINCIPLE AND FABRICATION PROCESS OF MET ACCELEROMETER

2.1 Structures MET Accelerometer

Solid- state inertial sensors with small size, low noise and high sensitivity have been developed for several decades which have been widely commercialized and made a huge impact. Basically, solid-state inertial transducer is based on the mass-spring system with suspended proof mass, which has complex fabrication and poor performance at low frequency response. Low frequency vibration signal exist almost everywhere in the environment which is essential to the seismology and resource detection in the oil industry. Resonant frequency of spring-proof mass system ω0 can be described with the spring constant k and equivalent mass m, which is

$$\omega_0 = \sqrt{k / m} \qquad (1).$$

As the result, to achieve a stationary performance at high frequency, reducing the quantity and increasing the spring constant would be applied at solid-state device with size reduction. On the contrary, low frequency response needs heavy proof mass, which is contradictory to achieve both a good performance at low frequency and small sized device with solid-state.

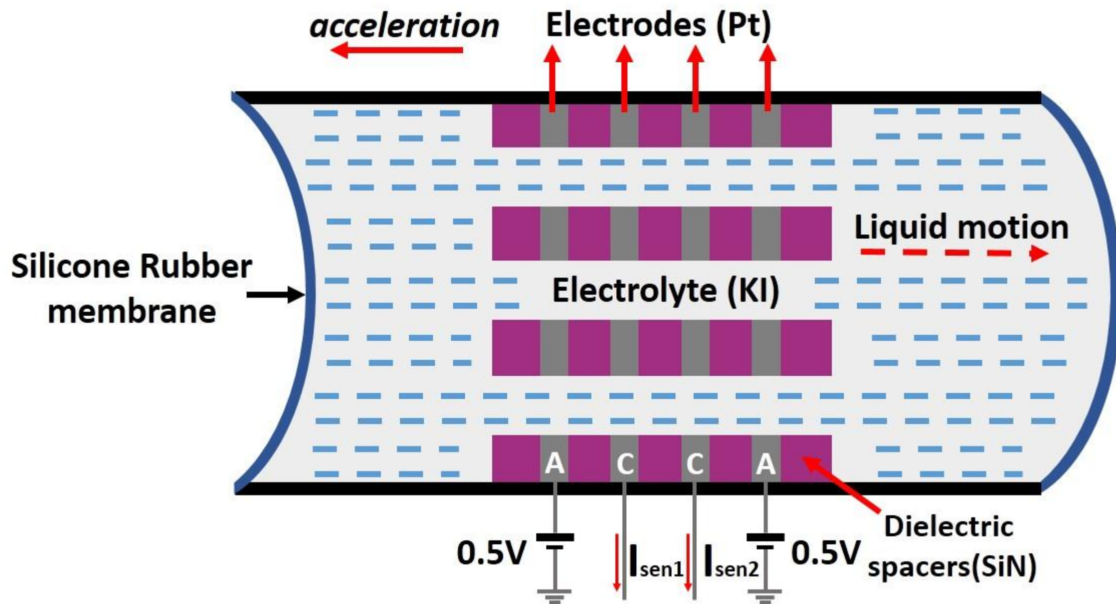

Figure 13 Traditional MET accelerometer

Comparing to the solid one, molecular electronic transducer (MET) is based on the liquid-state motion, which provide an alternative method to transform the vibration to electrical signal through the mass and charge transport with four fixed electrodes sensing the ionic liquid. [11]

The basic idea of the accelerometer structures using iodine-iodide solution as inertial mass is shown in Figure 13. Four electrodes distribute as anode-cathode-cathode-anode (A-C-C-A) which are separated by dialectic space layer which constituted a thin film diaphragm which is microporous for the liquid flowing. The diaphragm is sealed in a solid chamber with high-flexibility diaphragms (silicone rubber) capped at the portholes. Considering about the chemical durability in the ionic liquid, platinum is used as the electrodes and silicon nitride is chosen as the dielectric spacers. With 0.5V DC voltage exciting the two anodes, two differential current signals would be generated when the system is under vibration.

Although the design above is feasible, numbers of faults would limit the commercialization:

(1) High cost of manufacturing;

(2) Poor uniformity for one batch of devices;

(3) Poor sensitivity at high frequency;

(4) Self-noise control is difficult;

(5) Poor capability to CMOS manufacturing. [12]

Therefore, this work develops a new design with horizontal distributed electrodes instead of this 3D structure. Instead of chamber with membrane, the oil-encapsulated electrolyte droplet is dispensed on top of four parallel electrodes sealed with a minisize channel. Although the fundamental operation principle is similar to the 3D structure one, which the same voltage and peripheral circuits are applied, the spring force is applied by the oil seal rather than the rubber membrane. This would be discussed in chapter 2.2.

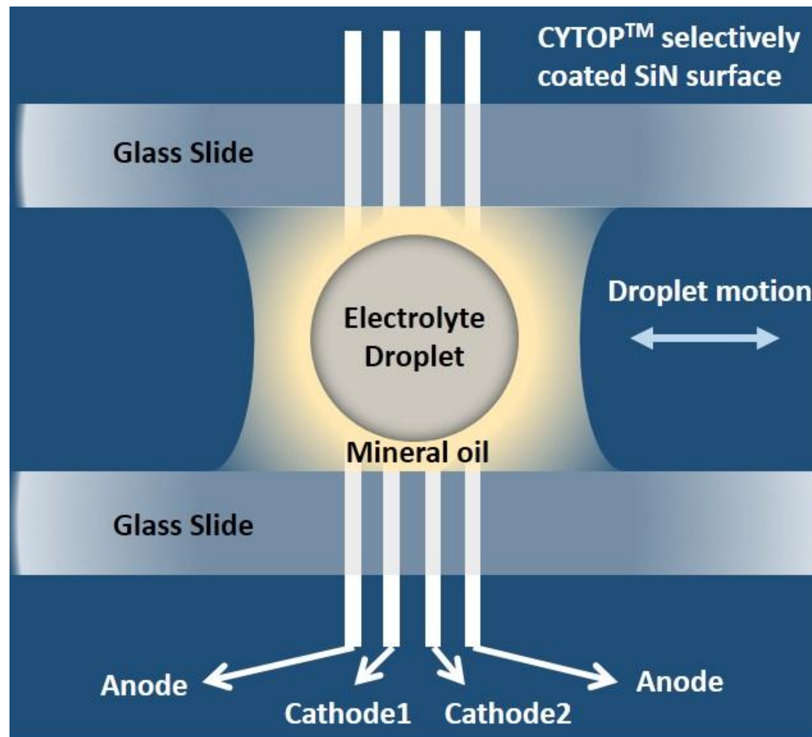

Figure 14 Droplet MET accelerometer

2.2 Principle of Droplet Movement

According to the Figure 14, if an external acceleration is applied to the frame of MET sensor, an inertial force will be applied on the electrolyte droplet. Once the droplet moves to the right through the channel, a hydrodynamic drag force would be applied oppositely. Assume $u(t)$ is the ground motion relative to the frame and $x(t)$ is the displacement from the droplet relative to the ground. Two forces will effect on the proof mass:

Restoring force from the oil seal, $-kV(t)$, opposes to the flow motion relative to the ground, where $V(t)$ is the volume of the droplet, k is the relative spring constant relative to the parameters and shape of the oil seal.

Damping force, $-R_h S_{ch} dV(t)/dt$, which is linearly proportional to the volumetric flow

rate of the droplet, in which Rh represents the hydrodynamic resistance which is negative and opposite to the liquid flow, S_{ch} represents the cross session area of channel.

The total acceleration is the acceleration respect to the ground d^2x/dt^2 and the ground acceleration $a(t)= d^2u/dt^2$. According to Newton second Law, The acceleration of a body is directly proportional to, and in the same direction as, the net force acting on the body, and inversely proportional to its mass according to which the equation describes the motion of droplet is:

$$-R_h S_{ch} \frac{dV(t)}{dt} - kV(t) = m\frac{d^2x(t)}{dt^2} + ma(t)\,. \quad (2)$$

With the relations of

$$V(t) = S_{ch}x(t)\,, m = \rho L S_{ch} \qquad (3)$$

Where m represents the mass, ρ is the electrolyte density, L is the length of the channel, Eq. (2) could be transformed to

$$\frac{d^2V(t)}{dt^2} + \frac{R_h S_{ch}}{\rho L}\frac{dV(t)}{dt} + \frac{k}{\rho L}V(t) = -S_{ch}a(t)\,. \quad (4)$$

Assume Q(t) is the volumetric flow rate, which Q(t)=dV(t)/dt. For the frequency domain, the transfer function of the droplet motion can be obtained as,

$$\left|H_{mesh}(\omega)\right| = \left|\frac{Q(\omega)}{a(\omega)}\right| = \frac{\rho L}{\sqrt{(\frac{\rho L}{S_{ch}})^2 \frac{(\omega^2 - \omega_0^2)^2}{\omega^2} + R_h^2}} \qquad (5)$$

where $\omega_0 = \sqrt{k / \rho L}$ is the mechanical resonant frequency of the device. According to the equations, the mechanical sensitivity and resonant frequency to the acceleration are relative to the spring constant k, properties such as the density, size and hydrodynamic

impedance of the ionic droplet.

2.3 Principle of Electrochemical Reaction

When a voltage is applied in the system as shown in the Figure14, electrochemical current which is also called "background current" [13] is independent of the mechanical motion. As the result, electrochemical reactions develops the concentration gradients of the solution components which leads the electrolyte diffusion of ions from one electrode to another as shown in the Figure 15 (a). When an acceleration is added on the frame, the relative displacement between the frame and the droplet will generate an additional convective transport of ions as shown in Figure 15 (b).

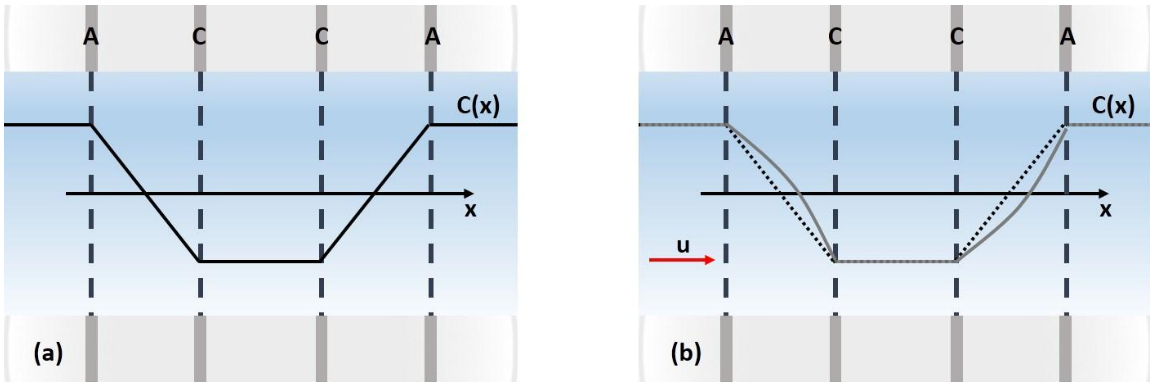

Figure 15 Distribution of the concentration of electrolyte

As the concentration of the ions on the surface of the electrodes the current between adjacent anode and cathode represents:

$$I = -Dq\oint_{S}(\nabla c ds) \qquad (6)$$

where, D is the diffusion coefficient, c is the concentration of charge carriers, q is the charge of carriers, S is the electrode surface area. As the result the differential of the cathodes would be

$$I_{out}(t) = I_{c2}(t) - I_{c1}(t) = Dq(\oint_{S_{c2}} (\nabla c, n) dS_{c2} - \oint_{S_{c1}} (\nabla c, n) dS_{c1})) \quad (7)$$

Where S_{c2} and S_{c1} are the surface are corresponding to the cathodes. Based on the Navier-Stokes equation and Nernst-Planck equation, an approximated expression of the electrochemical transfer function in the frequency domain between the current and volumetric flow rate is used

$$|H_{ec}(\omega)| = \left|\frac{I(\omega)}{Q(\omega)}\right| = \frac{C}{\sqrt{1+(\frac{\omega}{\omega_d})^2}} \quad (8)$$

where *C (A/(m3/s))* is the conversion factor of the electrochemical cell, $\omega_d = D/d^2$ is the diffusion frequency and d is the inter-electrode distance. As the result, the overall transfer function of MET droplet accelerometer can be written as,

$$|H(\omega)| = \left|\frac{I(\omega)}{a(\omega)}\right| = \frac{\rho L}{\sqrt{(\frac{\rho L}{S_{ch}})^2 \frac{(\omega^2 - \omega_0^2)^2}{\omega^2} + R_h^2}} \bullet \frac{C}{\sqrt{1+(\frac{\omega}{\omega_d})^2}} \quad (9)$$

2.4 Fabrication Process

As Figure 16 shows, there are 8 steps which are all under low temperature process except the LPCVD of silicon nitride. As the result, most processes can be provided after the CMOS fabrication which means the device has high capability to CMOS fabrication.

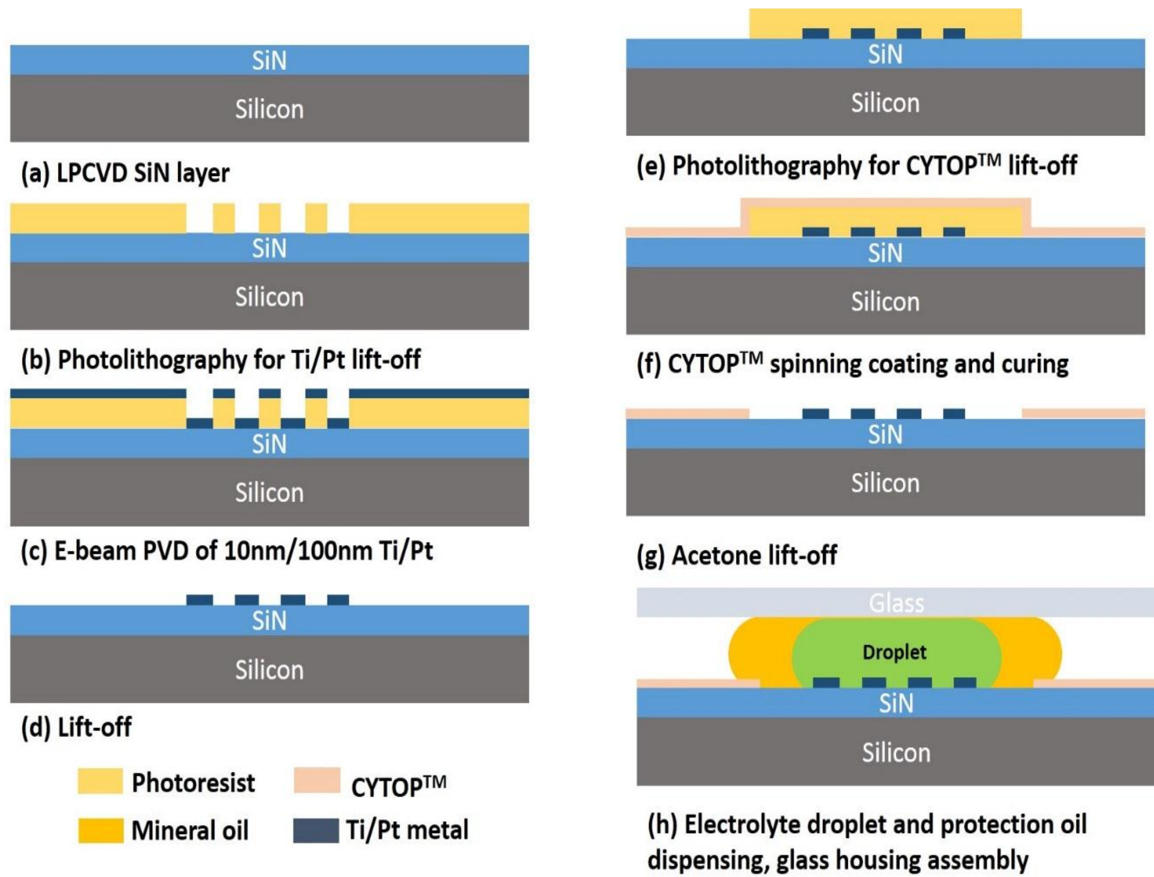

Figure 16 Fabrication Process Flow

Firstly, four electrodes made of Ti/Pt whose thicknesses are $10nm$ and $100nm$ are deposited using E-beam PVD and patterned with the width of $h = 100um$ and inter-electrode spacing of $d = 30\mu m$ by lift-off process. Then, surface modification is provided to reduce the hysteresis of droplet deformation which is exposed to oxygen plasma at *50 W* for *30 seconds* for surface hydroxylation. After that, the hydrophobic CYTOPTM thin film is coated on top to the silicon nitride surface without the four electrodes using lift-off again with certain pattern (hydrophilic spot surrounded by the hydrophobic areas). Afterwards, a $0.8\mu L$ concentrated iodine-iodide electrolyte droplet is sealed in the small amount of mineral oil which are sequentially dispensed by micropipettes in the hydrophilic

area covering platinum electrodes. The oil not only prevents the electrolyte droplet from evaporating, but also works as the elastic diaphragm to contain the electrolyte, which allows the droplet to be stabilized in the center. Finally, the glass housing channel with 1 mm in both width and height is assembled. The overview of the MET droplet accelerometer is shown in Figure 17.

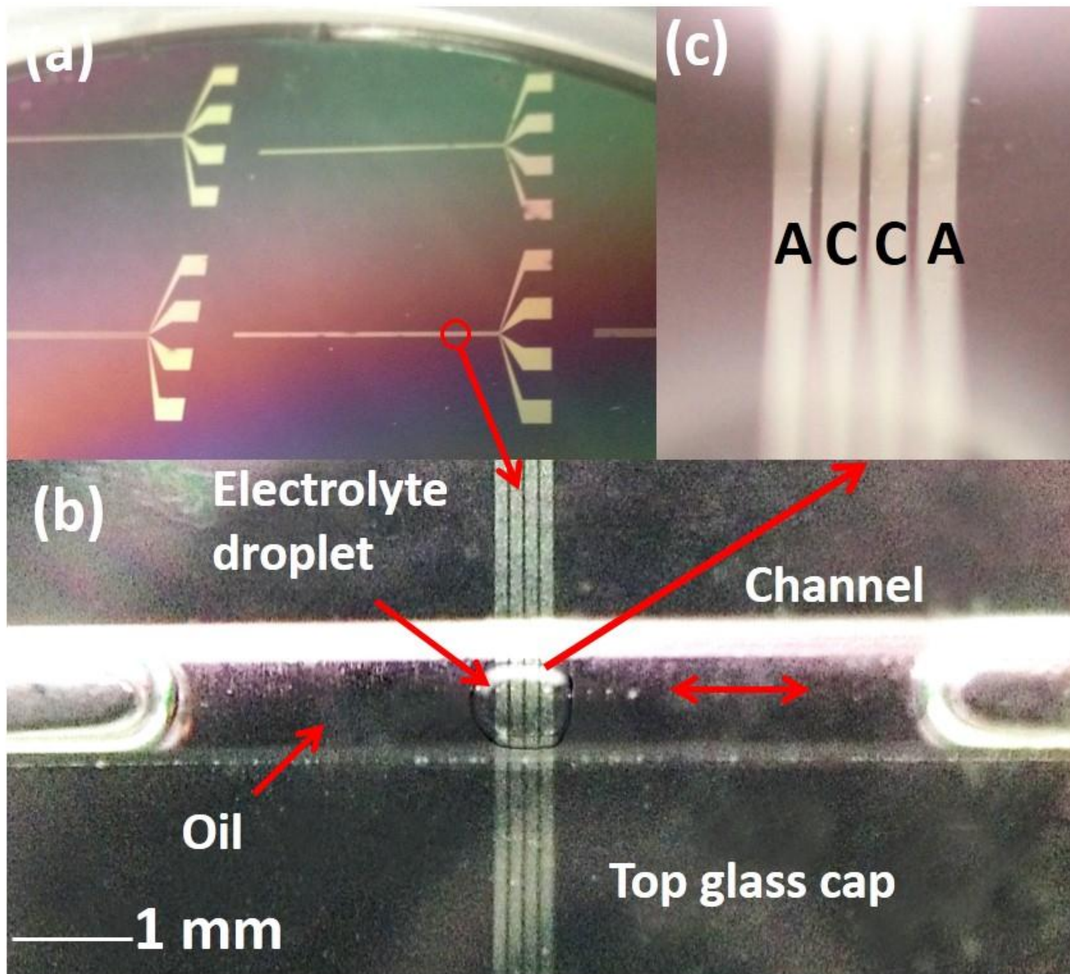

Figure 17 Overview of the electrolyte droplet-based MET accelerometer

Chapter 3

PERIPHERAL CIRCUITS DESIGN

3.1 Circuit Design for the Signal Analysis

According to the introduction of MET in the previous part, MET device is a DC-biased device, which means it needs a power supply. For this reason, it could be regard as a Voltage Source connect a variable resistance in series. Using the Norton theorem, the whole MET device equals to a current source connected with a resistance in shunt.

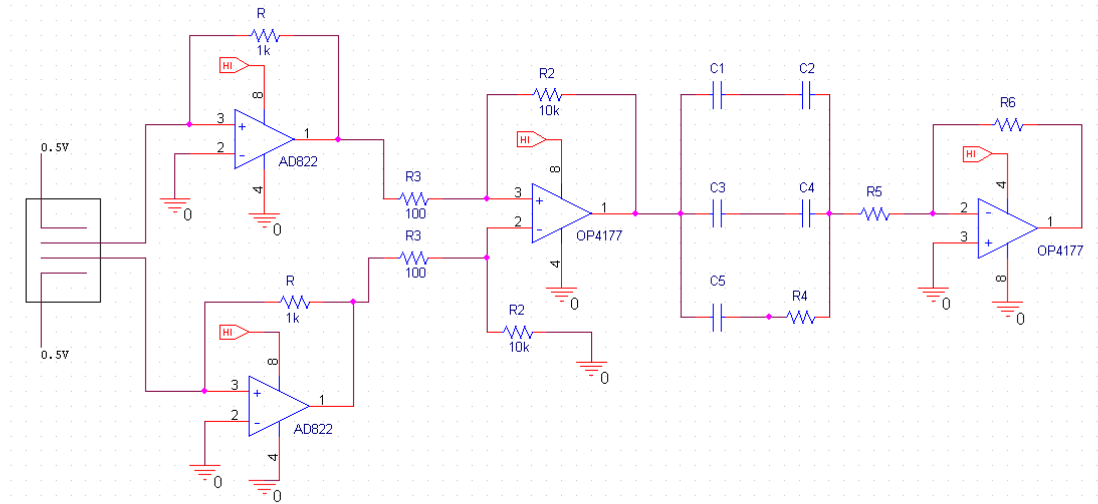

Figure 18 Schematic of peripheral circuit

With this conversion we can calculate the output current of MET is around $20 \sim 40\mu\text{A}$, which is hard to be detected. As the result, using a Current-Voltage amplifier is the way to detect the output. As the figure shown above, the positive pole of Amp connects to the ground and the negative pole connects to the output with a 1k resistance in series. The function of the amplifier is:

$$V_{out1} - 0 = -I_{in}R \quad (10)$$

According to the function above, the V_{out} is around $20 - 40\text{mV}$.

If the result is the acceleration or the sound pressure, the output needs to be a differential result of the 2 inputs. So that, the next step is to build a differential amplifier. R_2 is 100 ohms and R_3 is 10k ohms. As the Figure 18 shown above the function of the output is:

$$V_{out2} = (V_{in1} - V_{in2})\frac{R_2}{R_3} \qquad (11)$$

According to the function below, the DC gain of the electronics is:

$$\frac{V_{out3}}{\Delta I_{in}} = R \cdot \frac{R_2}{R_3} \qquad (12)$$

As the MET device only works between a specific frequency band, bandwidth filters need to be designed in the circuits. The C_1,C_2…C_5 and R_4 between the last two stages create LH poles and a RH zero which can filter the specific low frequency and the high frequency. The transfer function between the last two stages is

$$\frac{V_{out(filter)}}{V_{in(filter)}} = \frac{(s - x_1)}{(s + x_2)(s + x_3)} \qquad (13)$$

Thus, x_1, x_2 and x_3 mostly depend on the value of C_1, C_2…C_5 and R_4. The last stage is a negative amplifier which will amplify the signal again without amplifying the noise out of the bandwidth.

In order to measure the noise floor of the circuits itself, the two inputs connect to the ground. And due to the simulation of Labview, we use the FFT Power Density Function to measure the noise floor and result shows that from DC to 2k Hz, the noise floor is below -120 dB, which means the noise below 2k Hz is smaller than 10E-6 V. This result is acceptable to using the circuit to measure the MET device. If this circuit is integrated the noise will decrease a lot. The functionality of the electronic stages is the following:

a. Chip AD822 is a current to voltage convertor.

b. Chip OP4177 is a differential amplifier.

c. C1, C2…C5 and R4 compose a bandwidth filter.

In general, the design of the electronics is flexible and can be adjust with different kind of MET device.

3.2 Temperature Compensation

Generically, temperature compensation is the adjustment in performance of a system to compensate for changes in temperature. [14] In circuits design, it usually takes the form of a temperature-sensitive component connected as part of the active circuit or as part of a feedback loop. The operational transconductance amplifier (OTA) as a basic active element for the design of current-controlled or voltage-controlled filters and amplifiers, is appropriate to be a temperature compensation component connected in feedback loops.

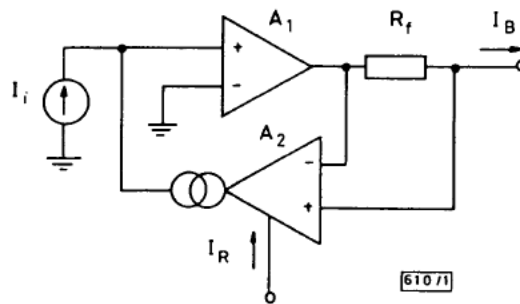

Figure 19 Biasing circuit for temperature compensation [14]

The design of the temperature compensation circuit is shown in the figure, in which A1 is an op-amp and A_2 is an OTA. With A_2 in the feedback loop of A_1 the current amplification I_B/I_i is oppositely proportional to A_2's transconductance. I_B is the bias current of OTA and I_R is constant. As the negative input of A_1 is a virtual earth note, voltage can

be controlled by the series resistor. The current gain of the circuit is given by

$$\frac{I_B}{I_i} = \frac{1}{g_m R_f}, \qquad (14)$$

Where gm is the transconductance of A2, given by

$$g_m = \frac{I_R}{2V_T} \qquad (15)$$

Where VT is the thermal voltage,

$$V_T = \frac{kT}{q} \qquad (16)$$

The transconductance gmB of the OTA biased by the IB output is given by

$$g_{mB} = \frac{I_i}{I_R R_f} \qquad (17)$$

Generally $g_{mB} = \frac{I_i}{I_R R_f} - \frac{I_R}{4\beta V_T}$ explains the second term in the above equation, the

temperature sensitivity of gmB is given, assuming β is constant, by

$$S_T^{g_{mB}} = \frac{\partial g_{mB}}{\partial T} \frac{T}{g_{mB}} = \frac{I_R}{I_i} \frac{I_R R_f}{4\beta V_T} \qquad (18)$$

If the I_R is low enough, the sensitivity will be low as well. And the $I_R R_f << 4\beta V_T$,

so that in a large range of current input, the sensitivity to the temperature will be small.

Chapter 4

TEST AND RESULTS

4.1 Test Setup

According to the circuits design discussed above, an instrument amplifier (AD620) is applied rather than the OP4117 in order to decrease the circuit's noise and increase the gain. With an integrated PCB board, as shown in the Figure 20, it is convenient to carry and assembling which we can embedded the MET device on a vibration stage with a reference accelerometer made by Analog Device (ADXL202).

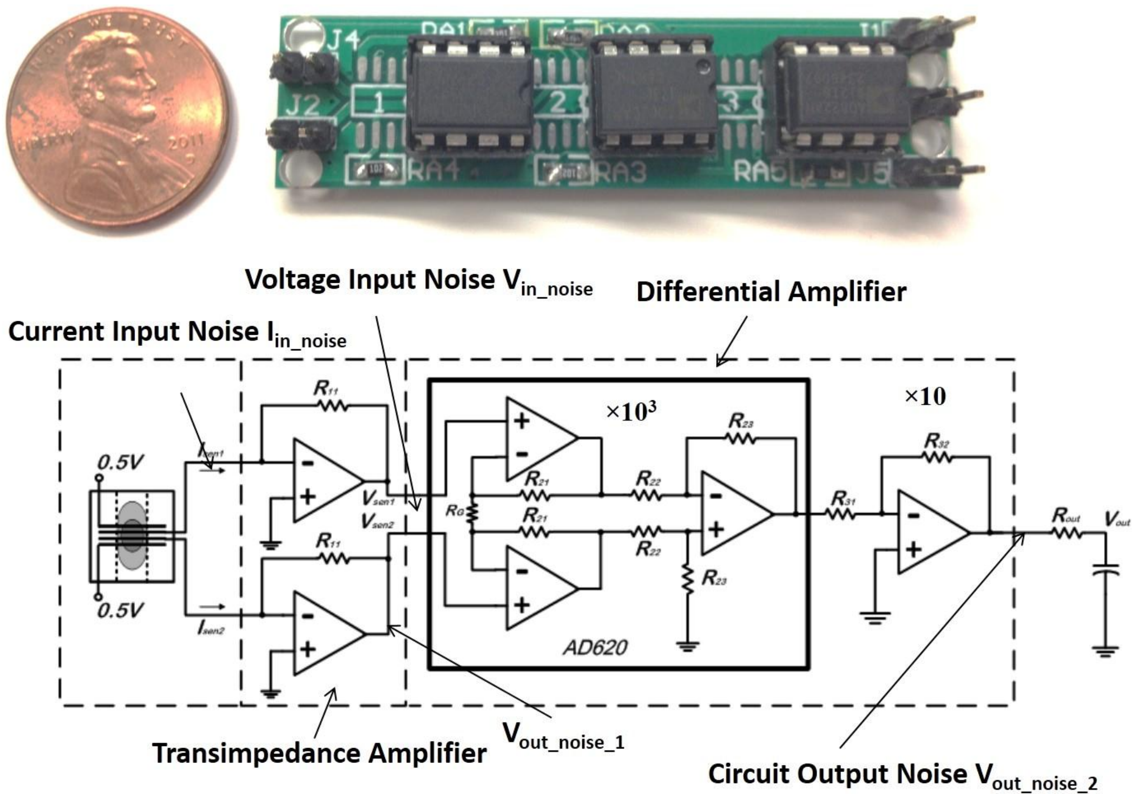

Figure 20 Overview of the PCB board

With a power amplifier connected to a signal generator (Smart Device) which can generate at least 1 Hz signal, signals from 1Hz to 2M Hz can be amplified which can excite

the vibration stage with low noise. As shown in the Figure 21, PCB board is setup isolated from the vibration area in order to cut out distraction. With Data Acquisition Card, vibration data can be recorded by the Labview and with FFT tool and sensitivity and resolution of the MET sensor can be calculated according to the time domain chart.

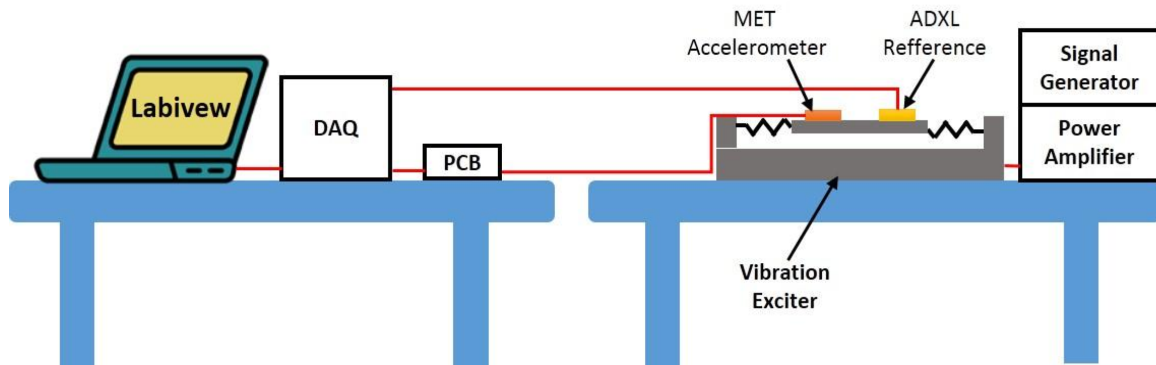

Figure 21 Test Setup Schematic

4.2 Experimental Results

Experimental results is conducted using a MET device with $d=30\ \mu m$, $h=100\ \mu m$. With tuning the gain of power amplifier, the acceleration of the vibration can be controlled which we can got a good linearity sensitivity. Figure 22 shows measured outputs in response to a 20 Hz sinusoidal acceleration between $\pm 0.6G$. The sensitivity achieves $10.8V/G$.

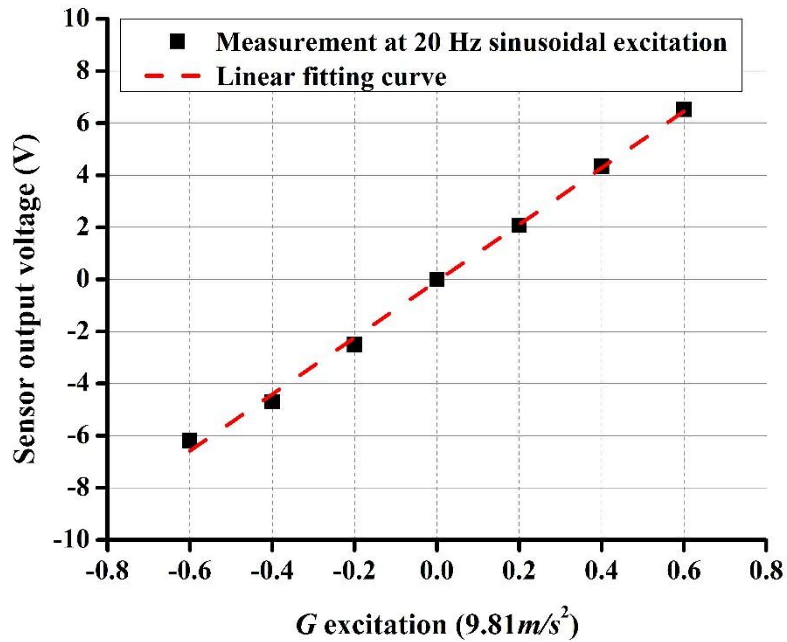

Figure 22 Measurement result of sensitivity of the MET accelerometer at 20 Hz

The sensor is then sequentially subjected to a series of excitations whose amplitudes are approximately constant (0.35G) covering 1-200 *Hz* frequency range. Figure 23 shows the measured sensitivity spectrum. It has nearly flat response in the frequency range of 1-40 *Hz*.

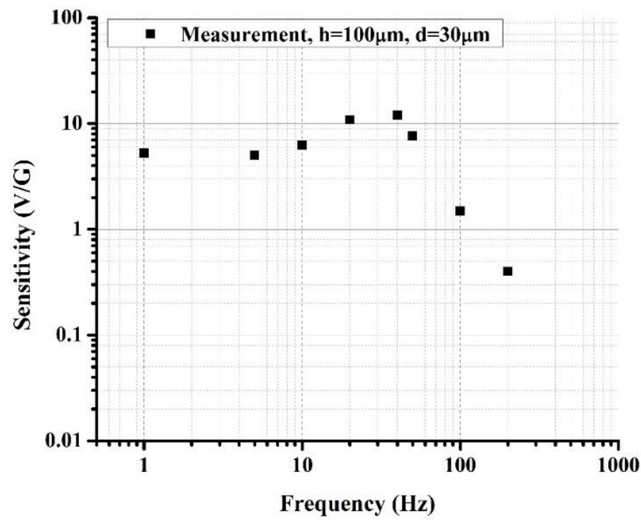

Figure 23 Measurement result of sensitivity frequency response of the droplet-based micro MET accelerometer

Figure 24 presents the measured spectrum of the accelerometer output under a 20 *Hz*, 0.35*G* sinusoidal acceleration. The equivalent input-referred noise floor is 100 μG/$\sqrt{Hz}$ at 20 *Hz*, given that the sensitivity is 10.8 *V/G* at 20 *Hz*.

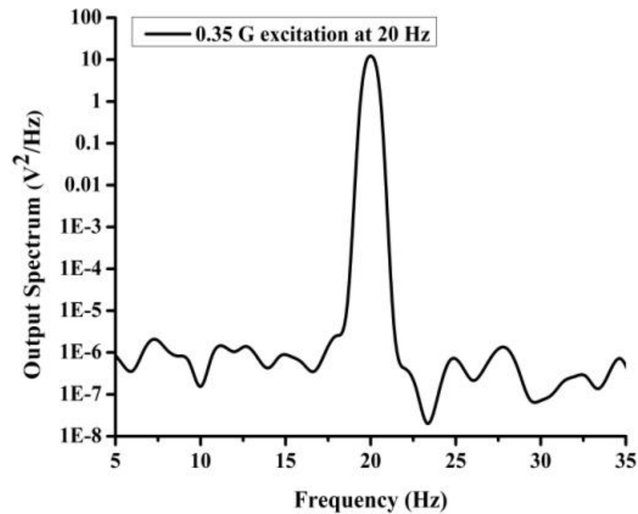

Figure 24 Measured output signal spectrum under a 0.35 G sinusoidal excitation at 20 Hz.

4.3 Noise Analysis and Improvement

As the result of the experiment, the sensitivity of the whole system is 10.8V/G. The noise-referred noise floor of the device is 100 $\mu G/\sqrt{Hz}$). The noise floor of the Device is shown in the Figure 24. The Noise floor of the Circuit tested by DAQ6008 (cheap one), tested by DAQ6289 (New one), the DAQ Card Limit (DAQ6008 cheap one) and the DAQ Card Limit (DAQ6289 New one) are shown in the Figure 25. The calculation of the Circuit noise floor is shown in Figure 21.

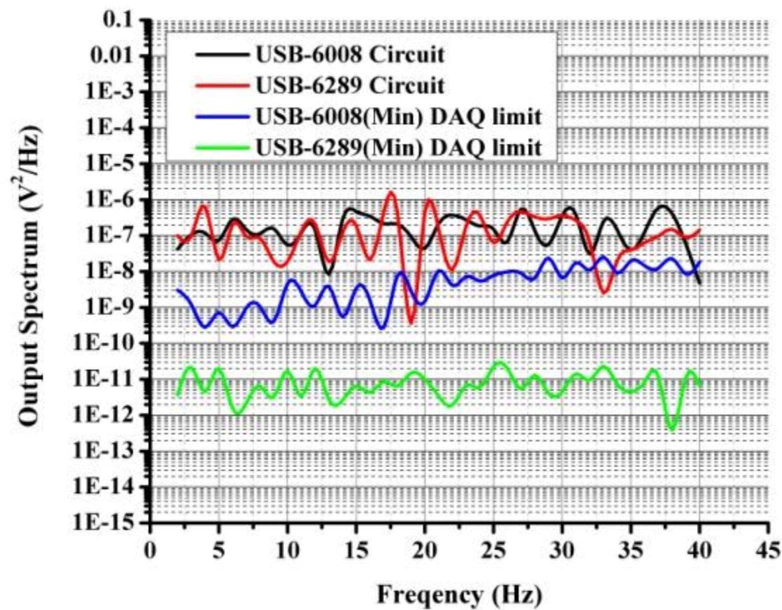

Figure 25 Noise spectrum of test Circuits.

Name	Output Spectrum($\mathbf{V^2/Hz}$)	Input-referred ($\mathbf{\mu G/\sqrt{Hz}}$)
Device	1E-6	100
Circuit Calculation	1.6 E-7	38.87
Circuit(DAQ6008)	3E-7	54.77
Circuit(DAQ6289)	3E-7	54.77
Read Limit(DAQ6008)	1E-8	10
Read Limit(DAQ6289)	1E-11	0.316

Table 2 Self noise analysis of test equipment

The input-referred value is according to total gain of 107 **Ω**. The transimpedance amplifier stage:

$$V_{out_noise_1} = I_{in_noise} \cdot R_{gain} = 20\ fA/\sqrt{Hz} \times 1\ k\Omega = 20\ pV/\sqrt{Hz} \qquad (19)$$

I_{in_noise} refers to the Current Input-referred noise of the AD822, which is around 20 fA/$\sqrt{Hz}$ around 10 Hz. R_{gain} refers to the gain of transimpedance amplifier, which is 1 kΩ.

The Differential amplifier stage:

$$V_{out_noise_2} = V_{in_noise} \cdot Gain = 40.04\ nV/\sqrt{Hz} \times 10^4 = 400.4\ \mu V/\sqrt{Hz} \qquad (20)$$

Gain refers to the gain of the differential amplifier, which is 10^4.V_{in_noise} includes the voltage input-referred noise of AD620 plus the $V_{out_noise_1}$. As, this is the differential structure, the total V_{in_noise} will be double, which is

$$(20\ nV/\sqrt{Hz} + 20\ fA/\sqrt{Hz}) \times 2 \times 10^4 = 400.4\ \mu V/\sqrt{Hz} \qquad (21)$$

As the sensitivity is 10.3 V/G, the circuit resolution refers to:

$$400.4\ \mu V/\sqrt{Hz} \div 10.3\ V/G = 38.87\ G/\sqrt{Hz} \qquad (22)$$

As the result of calculation above, the total gain of the measurement system is,

$$Gain_{total} = R_{gain} \cdot Gain = 1\ \mathbf{k}\Omega \times 10^4 = 10^7\Omega \qquad (23)$$

The primary noise source is the voltage input-referred noise of differential amplifier (AD620), as the current input-referred noise of transimpedance amplifier (AD822) is very low. To increase the total gain and decrease the output noise, the best way is to increase the gain of the transimpedance amplifier and decrease the gain of differential amplifier. The noise floor of power spectrum analysis with (DAQ6289), with which have the different gain shows in the table below.

Num	R_{gain} (I-V Amp)	Gain (Diff Amp)	R_{total} (Total gain)	Noise Floor	Input-referred Noise floor
1	1 kΩ	10^4	10^7 Ω	3×10^{-6} $\mathbf{V^2/Hz}$	54.77 $\mathbf{\mu G/\sqrt{Hz}}$
2	10 kΩ	10^4	10^8 Ω	3×10^{-6} $\mathbf{V^2/Hz}$	5.477 $\mathbf{\mu G/\sqrt{Hz}}$
3	100 kΩ	10^3	10^8 Ω	3×10^{-7} $\mathbf{V^2/Hz}$	1.732 $\mathbf{\mu G/\sqrt{Hz}}$

Table 3 Noise floor with different gain

According to the table, the total gain of Num 2 is 10 times larger than Num 1, however their noise floors are equal with increasing the gain of transimpedance amplifier and total gain of Num 3 is equal to Num 2, however the noise floor is 10 times lower than Num 2 with increasing the gain of transimpedance amplifier and decreasing the gain of differential amplifier.

REFERENCES

[1] Huang, H., Liang, M., Tang, R., Oiler, J., Ma, T., Yu, H. An Electrolyte Droplet-Based Low Frequency Accelerometer Based on Molecular Electronic Transducer. In Proceedings of the 17th International Solid-State Sensors, Actuators and Microsystems Conference and Transducers 2013, Barcelona, Spain, 16–20, June, 2013.

[2] Bryzek, J., Petersen, K., Mallon, J. R., Christel, L., & Pourahmadi, F. (1990).Silicon sensors and microstructures. Nova Sensor.

[3] Detlefs, B. (1999). MicroElectroMechanical Systems (MEMS), An SPC Market Study. System Planning Corporation, 1429.

[4] Partridge, A., Reynolds, J. K., Chui, B. W., Chow, E. M., Fitzgerald, A. M., Zhang, L., ... & Kenny, T. W.(2000).A high-performance planar piezoresistive accelerometer. Microelectromechanical Systems, Journal of, 9(1), 58-66.

[5] Roylance, L. M., & Angell, J. B. (1979). A batch-fabricated silicon accelerometer. Electron Devices, IEEE Transactions on, 26(12), 1911-1917.

[6] Senturia, S. D. (2001). Microsystem design (Vol. 3). Boston: Kluwer academic publishers.

[7] Petersen, K. E. (2000, June). Bringing MEMS to market. In Proceedings of Solid-State Sensor and Actuator Workshop, Hilton Head Island, South Carolina(pp. 60-64).

[8] Xia, Y., & Whitesides, G. M. (1998). Soft lithography. Annual review of materials science, 28(1), 153-184.

[9] Krishnamoorthy, U., Olsson III, R. H., Bogart, G. R., Baker, M. S., Carr, D. W., Swiler, T. P., & Clews, P. J. (2008). In-plane MEMS-based nano-g accelerometer with sub-wavelength optical resonant sensor. Sensors and Actuators A: Physical, 145, 283-290.

[10] Razavi, B. (2002). Dsign Of Analog Cmos Intgrtd Circuits. Tata McGraw-Hill Education.]

[11] Kozlov, V. A., Agafonov, V. M., Bindler, J., & Vishnyakov, A. V. (2006). Small, Low-Power, Low-Cost Sensors for Personal Navigation and Stabilization Systems. In Proceedings of the 2006 National Technical Meeting of The Institute of Navigation (pp. 650-655).

[12] Huang, H., Carande, B., Tang, R., Oiler, J., Dmitriy, Z., Vadim, A., & Yu, H. (2013, January). Development of a micro seismometer based on molecular electronic transducer technology for planetary exploration. In Micro Electro Mechanical Systems (MEMS), 2013 IEEE 26th International Conference on (pp. 629-632). IEEE.

[13] Krishtop, V. G., Agafonov, V. M., & Bugaev, A. S. (2012). Technological principles of motion parameter transducers based on mass and charge transport in electrochemical microsystems. Russian Journal of Electrochemistry, 48(7), 746-755.

[14] Malvar, H. S., & Luettgen, M. (1987). Temperature compensation of OTA-based filters and amplifiers. Electronics Letters, 23(17), 890-891.